Nonlinear resonant stimulation and no-feedback control of the wake behind a circular cylinder

Frank Ohle and Marc Lange
Institut für Angewandte Mechanik und Strömungsphysik, Georg-August-Universität, Bunsenstrasse 10, 37073 Göttingen, Federal Republic of Germany
(Received 27 February 1995; revised manuscript received 9 August 1995)

Recently the concept of a nonfeedback control has been developed, based on having an accurate model of the unperturbed system from which an appropriate driving force can be calculated. In this work the application of the nonlinear resonant stimulation concept of Reiser, Hübler, and Lüscher [Z. Naturforsch. Teil A **42**, 803 (1987)] and the nonfeedback control method of Hübler and Lüscher [Naturwissenschaften **76**, 67 (1989)] is experimentally investigated. The experimental system that is considered is the periodic wake behind a circular cylinder at low Reynolds numbers. It will be shown that successful control, i.e., an increase or decrease of the width of the wake region, can be achieved by using an external sound excitation. Both experimental results and numerical simulations based on a low-dimensional model reconstructed from experimental data are in a good quantitative agreement. In addition we discuss the physical properties of a stimulated wake flow and the general problems of the experimental application of the control to such flows. Furthermore, an experimental setup is proposed from which a higher efficiency for the wake control and the possibility to achieve all kinds of preselected dynamics, such as a total suppression of the wake flow, can be expected. The advantages of this type of model-based control, its physical interpretation, and its applicability to technical flows will be discussed in detail.

PACS number(s): 47.20.Ky, 05.45.+b

I. INTRODUCTION

In recent years different concepts have been developed to direct nonlinear or chaotic dynamical systems to a preselected or goal dynamics [1,2]. While extensive literature exists on the subject of linear control with and without feedback [3–5], little is known about its nonlinear counterpart [6]. In this paper we present a systematic experimental study of a nonlinear resonant stimulation, and the possibility of applying a nonlinear nonfeedback control to the periodic wake behind a circular cylinder.

The ability to stimulate or control the dynamics of a considered system to effect a desired change is a very important task, both in basic research as well as in applied engineering. Since a large variety of interesting dynamical systems are characterized by their nonlinearity, the most efficient control of such systems might be achieved by using sufficient nonlinear driving forces [1]. The fundamental methods of driving a nonlinear dynamical system in a prescribed way are the H method, developed by Hübler and Lüscher [1], and the OGY method developed by Ott, Grebogi, and Yorke [2]. The H method is based on a nonfeedback control mechanism, and has been applied numerically to well-known oscillators [7,8], to fully developed and transitional solutions of the Ginzburg-Landau equation as models for shear flows [9] and the cylinder wake [10], and experimentally to a damped mechanical oscillator [11] and to fluid mechanical systems such as jets and wake flows [12,13]. The OGY method is based on a feedback mechanism. Different types of modified OGY methods are applied to control a chaotic oscillating metal beam in a magnetic field [14], to stabilize a laser beam [15] or high periodic orbits of a diode resonator [16], to control cardiac chaos [17], and to control a driven pendulum and a driven bronze ribbon [18]. Since most dynamical systems in the real world are nonlinear, there are a large number of further applications for these control mechanisms. In this work, the H method is applied, because with this method a large variety of different goal dynamics can be chosen.

In general the nonfeedback control of nonlinear systems which exhibit complicated dynamics shows serious problems. In many complex systems the significant control parameters do not vary at a rate slow compared to the governing order parameters. Furthermore, experimental systems are more or less influenced by disturbances from the surroundings, e.g., pressure, temperature or humidity in the laboratory, which may change slightly during the experiments. Since the nonfeedback control theory relies on forecasting techniques which are based on a low-dimensional model (LDM) for the dynamics of the experimental systems, the derivation of such LDM's is very important. Unfortunately very often low-dimensional models cannot be derived from first principles. Therefore the analysis of systems that exhibit complex dynamics in the form of a low-dimensional attractor begins with a state space reconstruction of the dynamics [19]. Methods have been developed to construct models from this representation, which reproduce the dynamics on a low-dimensional attractor [20–26], i.e., if the trajectories have no double points in state space, an autonomous system of ordinary differential equations of the form

$$\dot{X}=\frac{dX}{dt}=f(X) \tag{1}$$

can be derived. Here X characterizes continuous variables $(x_1,\ldots,x_n)$ of the system, f is a matrix describing the generally nonlinear coupling among the variables, and t defines the time. Although not obtained from first principles, such a model can be used for dynamical system analysis [27], forecasting, and noise reduction [28], to resonantly stimulate a nonlinear system [7,29,30], or to direct a system to a preselected dynamics [1,2]. It is the nonlinear resonant stimulation and the control to a preselected dynamics we propose to investigate here. In general, both control procedures discussed in this paper are very simple. First, construct a LDM or improve the LDM after an unexpected change in the experimental system; and, second, implement the control by an appropriate driving force. This force results from a comparison of the LDM to the equation of motion of the goal dynamics. As long as the control parameters of the experimental system change slowly compared to the typical time scale of the experimental dynamics, the time between two succeeding improvements of the LDM may be long, and the control is basically an open-loop control [24].

A challenging question in fluid mechanics is still the active control of wake flows behind bluff bodies (see Ref. [31]). In the following we will investigate the possibility of resonant stimulation and nonfeedback control of such a wake to a preselected dynamics or goal dynamics. The experimental system considered here is the wake behind a circular cylinder in the periodic regime ($50\leq \mathrm{Re}=U_\infty d/\nu\leq 160$; U_∞ is the flow speed, d is the cylinder diameter, and ν is the kinematic viscosity). Since the basic equation of motion to describe the dynamical behavior of the vortex street are the Navier-Stokes equations, an accurate low-dimensional model must be derived. It has been shown elsewhere [32,33] that a LDM for the regular dynamics of the cylinder wake can be extracted from measured time signals. This model was a two-dimensional third order differential equation of the type

$$\ddot{u}=\sum_{\substack{i=0,\ldots,3\\ j=0,\ldots,3-i}} a_{ij}u^i\dot{u}^j, \tag{2}$$

where u denotes the instantaneous velocity component in the mean flow direction, $\dot{u}$ and $\ddot{u}$ are its first and second time derivatives, and a_{ij} are the coefficients of a Taylor series expansion. From this model the response to sinusoidal and nonlinear driving forces can be predicted, and the nonlinear control mechanism therefore possibly be applied with success [10,13].

In this paper we will investigate the extent to which the nonlinear resonant control mechanism [29,30] and the nonlinear nonfeedback control can be applied to the periodic cylinder wake. After the experimental setup is described, the basic principles of the nonlinear resonance stimulation of a dynamical system and the application to the vortex street is presented in Sec. III. Then in Sec. IV the nonfeedback control method is introduced, and the results from the experimental investigation are discussed. The problems concerning the transfer of the calculated driving forces by an external sound excitation are discussed in Secs. V and VI. Furthermore, the idea of an experimental arrangement for the control of the cylinder wake which might increase the efficiency of the wake control is proposed. Finally, in Sec. VI the physical insight and an outlook of the applicability of the nonlinear model-based control to technical flows at higher Reynolds numbers are presented.

II. EXPERIMENTAL SETUP

The measurements were carried in an open-circuit-type wind tunnel shown in Fig. 1. The wind tunnel is driven by a Thyristor-controlled direct current engine which is able to create velocities up to 28 m/s. The nozzle was especially designed to achieve laminar homogeneous flow in the core of the jet for low free stream velocities, in particular less than 3 m/s [34]. To achieve a low turbulence level at about 0.1%, a honeycomb, a special designed cone, and three riddles of different wire meshes have been used.

A circular stainless-steel cylinder with a diameter $d=1.5$ mm had a polished surface, and was mounted horizontally directly at the nozzle exit of 180-mm diameter. The cylinder and wind tunnel were separated to avoid any coupling. Furthermore, the cylinder was under mechanical tension to prevent vibrations, which might disturb the separation of the wake flow. A hot-wire

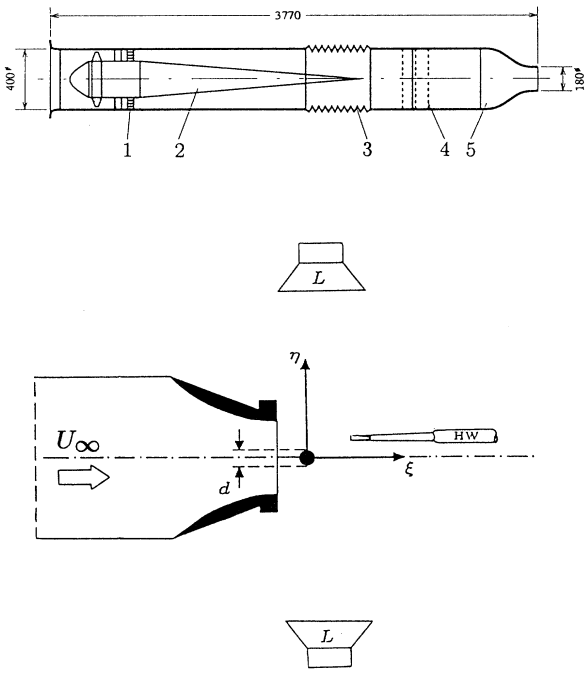

FIG. 1. Top: Schematic presentation of the wind tunnel; (1) honeycomb, (2) special designed cone to stabilize the flow, (3) PVC connecting piece, (4) three riddles of different wire meshes, and (5) nozzle. Bottom: test section. HW: hot-wire probe. L: loudspeakers. U_∞: mean stream velocity. d: cylinder diameter.

probe was placed halfway between the suspension points of the cylinder in the wake at downstream locations $\xi=3d$ and $\eta=d$ to one side to measure the velocity fluctuation. The origin of the coordinate system (ξ,η) coincides with the axis of the cylinder. The velocity signal was amplified, digitized by a 12-bit A/D converter, and sampled at 10 kHz. Two loudspeakers working 180° out of phase were placed outside the flow directly above and below the cylinder to superimpose sound.

III. NONLINEAR RESONANT STIMULATION

Resonant stimulation of oscillatory systems is a well-known process in engineering and applied physics. In this context the notion of resonance is defined by the largest response of a driven damped linear oscillator. A measure of the response of such a stimulated oscillator can be defined by the energy transfer

$$\Delta E=\int_0^T\left[F(t)\frac{du}{dt}\right], \tag{3}$$

where $F(t)$ is the time-dependent driving force, and T defines the time interval of the stimulation. In this case of a linear oscillator at resonance, the driving frequency of an external sinusoidal forces matches the natural frequency of the oscillator, yielding the largest energy transfer [30]. In the case of nonlinear oscillators, which are characterized by an amplitude-frequency coupling, resonant forcing is much more complicated. In general the eigenfrequencies of such systems are not defined, since their values depend on the amplitude. Recently it has been conjectured that a large energy transfer ΔE to nonlinear dynamical systems can be achieved by a special class of aperiodic driving forces [7,30]. It was shown elsewhere that an optimal control of nonlinear quantum systems verifies this observation [35].

In this section the idea of nonlinear resonant stimulation will be applied experimentally. In general the optimal resonant driving forces needed can be calculated by the following two methods.

In method I, the control signal $F(t)$ is calculated by

$$F(t)=(w_{01}-a_{01})\dot{u}_G\ , \tag{4}$$

where the term $w_{01}\dot{u}_G$ belongs to a model defined by the preselected or goal dynamics of the type

$$\ddot{u}_G=\sum_{\substack{i=0,\ldots,3\\ j=0,\ldots,3-i}} w_{ij}u_G^i\dot{u}_G^j\ . \tag{5}$$

The variable u_G denotes the preselected instantaneous velocity component in the mean flow direction, $\dot{u}_G$ and $\ddot{u}_G$ are its first and second time derivatives and w_{ij} are the preselected model coefficients. The expression of the control signal [Eq. (4)] represents the generalized definition of the notion of resonance in case of the resonant stimulation [7].

In method II, the control signal $F(t)$ is calculated from the time-reflected transient dynamics of the considered oscillator. From a mathematical point of view, this behavior corresponds to a change of the sign of the model equation terms $u^i\dot{u}^j$ with $j\neq 0$, i.e.,

$$F(t)=-\sum_{\substack{i=0,\ldots,3\\ j=0,\ldots,3-i}} w_{ij}u_G^i\dot{u}_G^j \quad \text{for } j\neq 0\ . \tag{6}$$

This forcing function reveals that nonlinear oscillators react most sensitively to their own transient dynamics [30]. More details about methods I and II can be taken from Refs. [7,30].

In the following, both methods will be applied to the periodic vortex streets behind a circular cylinder. Method I will be used for an increase of the velocity amplitude $u(t)$, i.e., an increase of the width of the wake region, whereas method II will be used for a decrease. The opposite application of these methods lead to similar results [10].

Nonlinear resonant stimulation of the vortex street

1. Increase of the width of the wake region

First the vortex streets is stimulated resonantly by the use of method I [Eq. (4)]. The aim is to increase the velocity amplitude $u(t)$ of the cylinder wake. Therefore the resonant control signal is calculated from

$$F(t)=\sigma|a_{01}|\dot{u}_G\ , \tag{7}$$

where

$$\sigma=\left[\frac{w_{01}}{a_{01}}-1\right]\mathrm{sgn}(a_{01}) \tag{8}$$

is the control parameter. By the use of such a control parameter σ, the energy transfer is given by

$$\Delta E=\int_0^T\left[F(t)\frac{du}{dt}\right]dt\begin{cases}>0 & \text{for } \sigma>0\\ =0 & \text{for } \sigma=0\\ <0 & \text{for } \sigma<0.\end{cases} \tag{9}$$

A systematic investigation of the cylinder wake is carried out at Re=67. Figure 2 shows the resonant stimulation of the vortex street (top), the numerical prediction from the extracted low-dimensional model [Eq. (2)] (middle), and the applied control signal calculated from Eq. (7) (bottom). The control parameter chosen was $\sigma=0.007$. In both presentations, i.e., the experimental and the model system, an increase in amplitude can be obtained. A distinctive feature of both driven systems is the asymmetry between the numerical and experimental time signals. The mean value of the experimental time signal is shifted to a lower mean velocity, whereas the numerical is shifted to a higher velocity. This deviation is based on a physical process of the wake flow, which is not considered in the numerical simulation. An increase in amplitude of the velocity fluctuation corresponds to an increase of the separated vortices and therefore the width of the wake region.

The global structure of such a wake flow is illustrated in Fig. 3, where a schematic representation of the mean velocity profile behind the cylinder for the natural and driven wake flows is presented. It can be seen that due to

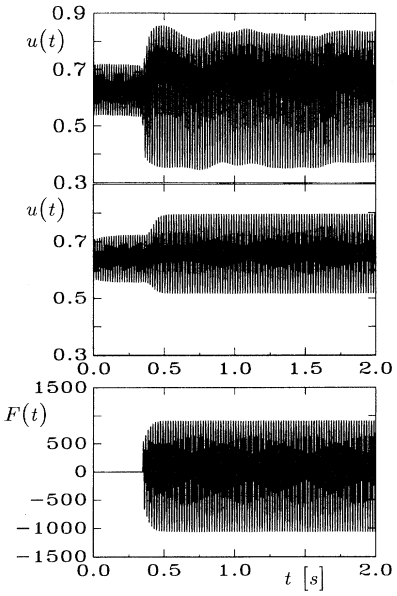

FIG. 2. Experimental (top) and simulated time signal from Eq. (2) (middle) of a resonantly stimulated vortex street at Re = 67. The goal was an increase in the velocity amplitude $u(t)$, i.e., an increase of the width of the wake region. The control signal $F(t)$ (bottom) was calculated from Eq. (7), where $\sigma=0.007$.

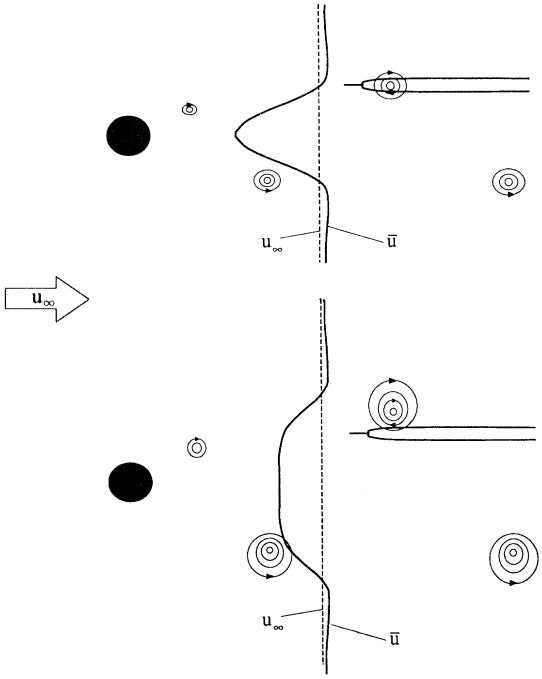

FIG. 3. Schematic presentation of the mean velocity profile of the wake region behind the cylinder. Top: natural state, bottom: stimulated state of a cylinder wake.

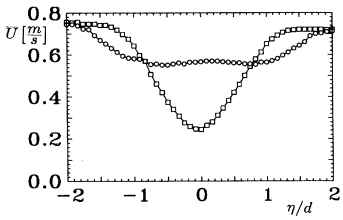

FIG. 4. Mean velocity profile vs the normalized probe position η/d for the natural (□) and the resonant stimulated vortex street (○) for the same experimental resonantly driven state shown in Fig. 2. The probe position behind the cylinder is $\xi/d=3$.

an increase in amplitude, the fixed probe position at a local point in space (ξ,η) moves relative to the vortices at the center of the wake, which causes a variation in mean velocity. This process is quantitatively verified in Fig. 4, where the mean velocities of natural and driven wake flows are measured for different η locations of the probe. In addition to a continuous change in mean velocity, the velocity amplitude is also dependent on the position (ξ,η) of observation. This statement is confirmed in Fig. 5, where it is shown that the increase of the velocity amplitude $A_c(\eta)=\frac{1}{2}|\max(u_c(t,\eta))-\min(u_c(t,\eta))|$ depends on the η coordinate normalized with the natural amplitude $A_{nc}(\eta)=\frac{1}{2}|\max(u_{nc}(t,\eta))-\min(u_{nc}(t,\eta))|$, i.e.,

$$A^*(\eta)=\frac{A_c(\eta)}{A_{nc}(\eta)}=\frac{\frac{1}{2}|\max(u_c(t,\eta))-\min(u_c(t,\eta))|}{\frac{1}{2}|\max(u_{nc}(t,\eta))-\min(u_{nc}(t,\eta))|}\,. \tag{10}$$

Note that for the control experiments the fixed probe position was always $\xi/d=3$ and $\eta/d=1$, i.e., an increase of the width of the wake region causes an increase in mean velocity and velocity amplitude.

In the last numerical experiment (Fig. 2) a sudden jump from the natural to the goal amplitude was investigated. The response of the vortex street to a continuous variation of the control parameter is shown in Fig. 6. The time-dependent control parameter $\sigma(t)$ is calculated from

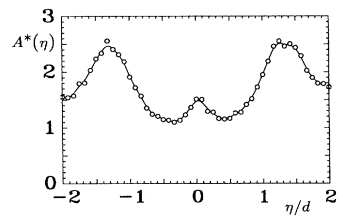

FIG. 5. Increase of the normalized amplitude A^* vs the normalized probe position η/d for the same experimental resonant driving shown in Fig. 2. The probe position behind the cylinder is $\xi/d=3.0$.

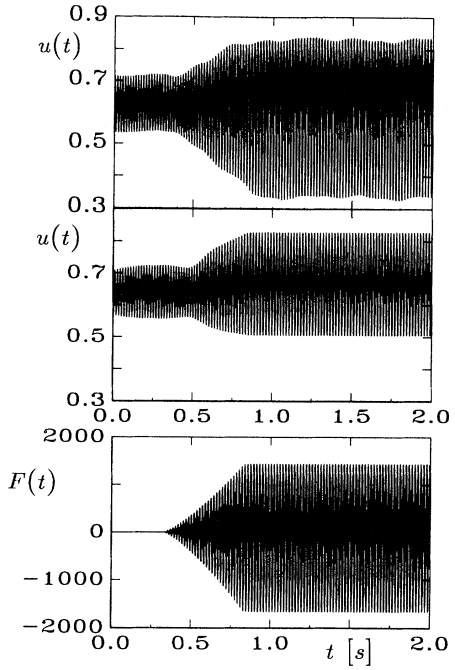

FIG. 6. Experimental (top) and simulated time signal from Eq. (2) (middle) of a resonantly stimulated vortex street at Re = 67. The control signal $F(t)$ (bottom) was calculated from Eq. (7), but here a time dependent control parameter $\sigma(t)$ was used [Eq. (11)]. $\sigma(t)=\max(\Delta\sigma,\sigma_{\mathrm{End}})$, $\Delta\sigma=0.002(\Delta t/s)$, and $\sigma_{\mathrm{End}}=0.001$.

$$\sigma(t)=\begin{cases}0 & \text{for } t<t_{FA}\\ \max(\Delta\sigma,\sigma_{\mathrm{End}}) & \text{for } t_{FA}\le t<t_{FE}\end{cases}, \tag{11}$$

where

$$\Delta\sigma=0.002\frac{t-t_{FA}}{s} \quad \text{and} \quad \sigma_{\mathrm{End}}=0.01 ,$$

and t_{FA} and t_{FE} define the time interval of the control. Taking the physical behavior of the stimulated vortex street introduced into account, a good agreement between the experimental system (Fig. 6, top) and the numerical simulation (middle) from the constructed model can be found. These results have also been obtained in flow visualization using the smoke-wire technique.

2. *Decrease of the width of the wake region*

Now we want to decrease the velocity amplitude of the vortex street, i.e., the width of the wake region by using method II. In this case, the control signal results from a reflection in time of the transient dynamics of the vortex street. A generalization of this type of control signal [Eq. (6)] by the introduction of a control parameter α then yields the relation

$$F(t)=(\alpha-1)\sum_{\substack{i=0,\ldots,3\\ j=0,\ldots,3-i}} w_{ij}u_G^i\dot{u}_G^j . \tag{12}$$

Figure 7 shows the numerical simulation of a vortex street stimulated with such force, and the applied control

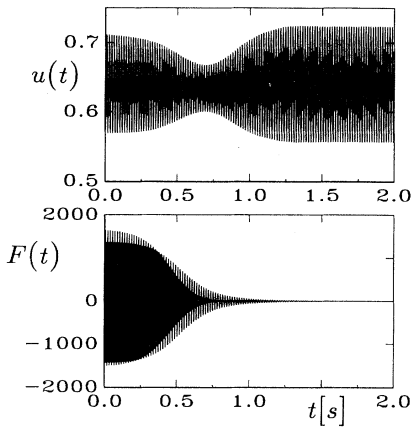

FIG. 7. Simulated time signal of a resonantly stimulated vortex street at Re = 67 (top) and the respective control signal $F(t)$ (bottom). Here the goal was defined by a decrease of the velocity amplitude $u(t)$.

signal calculated from Eq. (12) for $\alpha=-1$. The phases of $F(t)$ and $u(t)$ at the starting point of the control t_s are nearly similar, i.e., $\Delta\varphi\approx 0$. Because of these initial conditions, the system immediately locks into the goal dynamics. Therefore the frequency and the amplitude are entrained to lower values and, due to the amplitude-frequency coupling, a continuous decrease in amplitude can be obtained. When the control signal becomes too small, the oscillator unlocks from the driving force and converges back to its natural amplitude. However, the

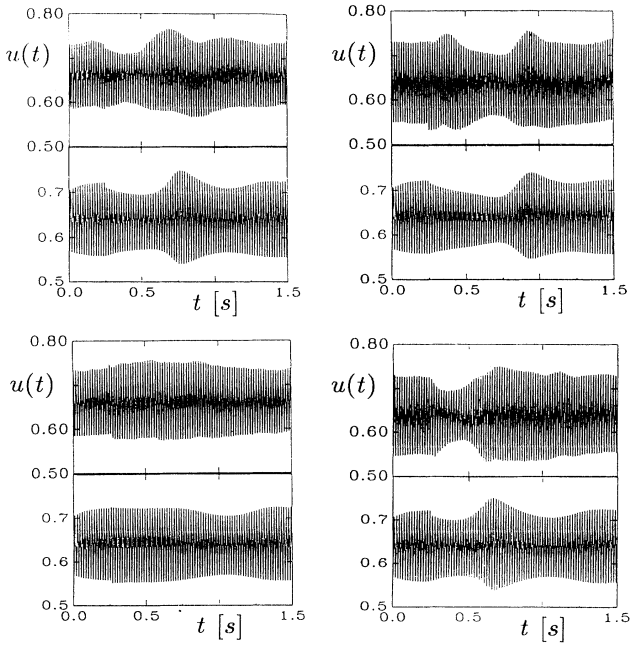

FIG. 8. Same as Fig. 7, but here a comparison of experimental time signal and numerical simulation from Eq. (2) for various phase differences $\Delta\varphi$ is shown. Experimental time signal (top) and numerical simulation (bottom).

control signal converges to zero and therefore only a decrease for a finite time is achieved. This result is also obtained for the experimental system. In the experiments the initial phase difference $\Delta\varphi$ at $t=t_c$ between the oscillator $u(t_c)$ and the control signal $F(t_c)$, where t_c is the starting point of the driving, cannot easily be determined. Due to the short time influence of the control signal, a number of different $\Delta\varphi$-dependent responses of the vortex street are possible. This statement is illustrated in Fig. 8, where for four different initial phase differences the experimental results for the vortex street at Re=67 and the corresponding numerical simulations from Eq. (2) are presented. The control signal was calculated from Eq. (12), where $\alpha=-1$. It is found that experimental results and numerical simulation are quantitatively in very good agreement. These results indicate that it might be possible to achieve a long time reduction of the velocity amplitude by the use of a modified control signal.

Because we do not want to lose the dynamical information of physical properties about the system like the amplitude-frequency coupling [Eq. (6)], a control function of the following type is constructed: if $F_A(t)$ is the initial control signal calculated from Eq. (12), then the modified driving signal reads

$$F(t)=\begin{cases} F_A(t) & \text{for } t>t_0 \\ F_A(t-nt_{AL}) & \text{for } t_0+nt_{AL}\le t<t_0+(n+1)t_{AL} \text{ with } n=0,2,4,\ldots \\ F_A[2t_0+(n+1)t_{AL}-t] & \text{for } t_0+nt_{AL}\le t<t_0+(n+1)t_{AL} \text{ with } n=1,3,5,\ldots . \end{cases} \tag{13}$$

The length of the starting interval, t_0, and the length of the remaining part intervals, t_{AL}, can be chosen under the conditions that $F_A(t_0+nt_{AL})$ with $n\in N$ possesses local maxima. In practice this was achieved in such a way that the computer program which calculates the control signal $F(t)$ automatically fits the preselected values for t_{AL} to the next maximum. In Fig. 9 such a control signal calculated from Eqs. (12) and (13) is presented. The numerical simulation of the application of such a driving force to the vortex street at Re=67 is shown in Fig. 10. The control signal is similar to Fig. 9, but here the control is switched on at $t_{FA}=1.5$ s and switched off at $t_{FE}=10.5$. The application of this force contains some interesting results in the dynamical behavior. First, at the beginning of the control the observed dynamical behavior is similar to Fig. 8, i.e., due to the amplitude-frequency coupling, a decrease of the amplitude for a finite time is found. Second, due to the modulation of the control signal, a complex response of the stimulated system can be obtained. Finally, these complex dynamics decay periodically in time and at about $t=7.0$ s the goal dynamics is achieved. After the control at $t=10.5$ s is switched off, the system converges back to its natural dynamical state. The corresponding experimental time signal is plotted in Fig. 11. A very good quantitative agreement between the experimental response and the numerical predictions (Fig. 10) is found. The decrease in amplitude and the corresponding reduction of the wake region have also been observed in the flow visualization. The maximal reduction of the amplitude found in both the experiments and the numerical simulation is at about 15% of the natural undisturbed amplitude. In general this maximal decrease in amplitude depends on the physical properties of the investigat-

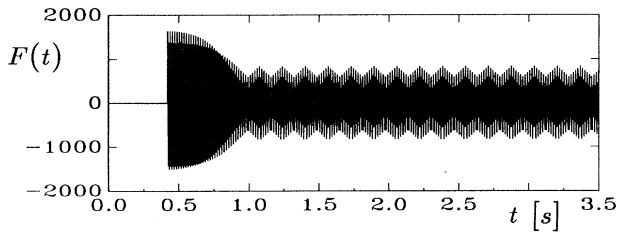

FIG. 9. Modified control signal $F(t)$ calculated from Eqs. (12) and (13), which will be used for a longtime decrease of the velocity amplitude $u(t)$.

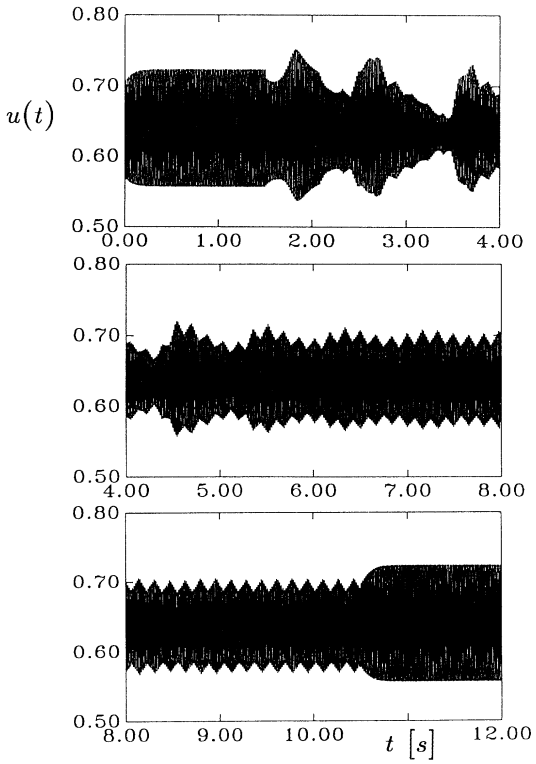

FIG. 10. Numerical simulation of a resonant stimulated vortex at Re = 67, where the force of Fig. 9 is applied. $t_{FA}=1.5$ s and $t_{FE}=10.5$ s.

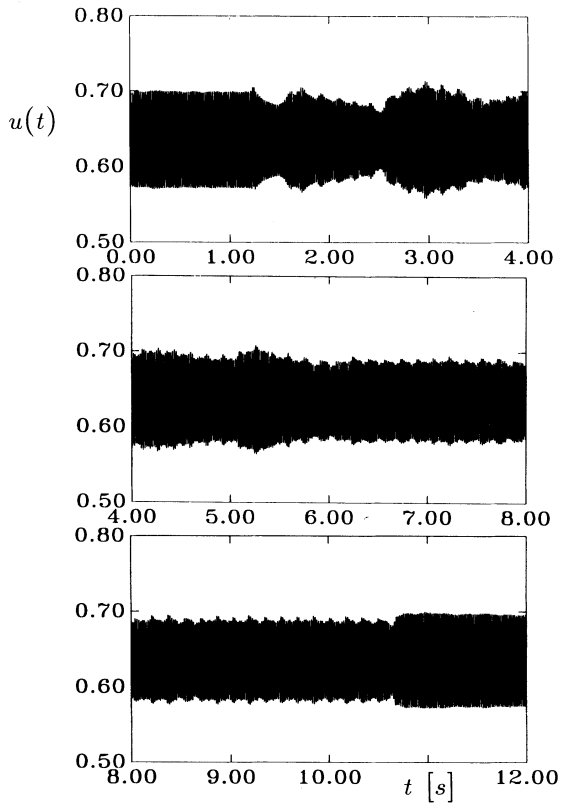

FIG. 11. Same as Fig. 10, but here the corresponding experimental time signal of a resonant stimulated vortex at Re = 67 using the force from Fig. 10 is presented. Here $t_{FA}=1.25$ s and $t_{FE}=10.65$ s.

ed oscillator.

The experimental and numerical results for the nonlinear resonant stimulation presented so far show a good quantitative agreement. Therefore one can expect a similar agreement for the nonfeedback control to a preselected or goal dynamics. The advantage of the nonfeedback control mechanism is the choice of a large number of possible goal dynamics such as stationary, periodic, or other dynamical states [7,10].

IV. NONFEEDBACK CONTROL

The basic principle of the no-feedback control mechanism developed by Hübler and Lüscher [1] is based on the following idea: Assume that an experimental system can be described by a differential equation of the type

$$\dot{\vec{x}}(t)=\vec{E}(\vec{x},t)+\vec{F}(t) , \tag{14}$$

where $\vec{F}(t)$ defines the driving force. If an exact equation is unknown or cannot be solved, a low-dimensional model

$$\dot{\vec{y}}(t)=\vec{M}(\vec{y},t) \tag{15}$$

must be determined, which describes accurately the dynamics of the experiment. In addition, a desired behavior of the systems is specified by the preselect dynamics

$$\dot{\vec{z}}(t)=\vec{G}(\vec{z},t) . \tag{16}$$

Then the appropriate driving force

$$\vec{F}(t)=\vec{G}(\vec{z},t)-\vec{M}(\vec{z},t) \tag{17}$$

can be calculated. For $\vec{x}(t)=\vec{z}(t)$ and $\vec{M}(\vec{y},t)=\vec{E}(\vec{x},t)$ the experimental system immediately locks into the goal dynamics $\vec{z}(t)$, and the control is accomplished. The most crucial point of this method is that if Eq. (14) is unknown or cannot be solved, then a model of the system dynamics [Eq. (15)] is needed. Such a model can be constructed, for example, from measured time signals [19–26]. With the nonfeedback control mechanism of Hübler and Lüscher [1] it is possible to select a large variety of different prescribed dynamics such as stationary solution (fixed point dynamics), periodic solutions, etc. In the case of the vortex street, this statement means that, from a mathematical point of view, a total suppression, i.e., the stabilization of the unstable stationary solution, might be possible.

No-feedback control of the vortex street

To control the vortex street without feedback to a preselected dynamics, a driving force of the type

$$\vec{F}(t)=\vec{G}(\vec{u}_G,t)-\vec{M}(\vec{u}_G,t) , \tag{18}$$

where $\vec{M}(\vec{u}_G,t)\approx\vec{E}(\vec{u}_G,t)$, must be calculated. Here $\vec{M}(\vec{u},t)$ represents the approximate model equation for the dynamics of the vortex street, and $\vec{G}(\vec{u}_G,t)$ is the goal dynamics. Since the model is of the type of Eq. (2), the general form of the driving force can be written as

$$F(t)=\sum_{\substack{i=0,\ldots,3\\ j=0,\ldots,3-i}} (w_{ij}-a_{ij})u_G^i\dot{u}_G^j . \tag{19}$$

In general, it is sufficient to vary just a subset of the coefficients w_{ij}. If only one coefficient is varied, Eq. (19) is simplified to

$$F(t)=(w_{ij}-a_{ij})u_G^i\dot{u}_G^j . \tag{20}$$

Now to simplify further discussions, a control parameter

$$\beta_{ij}=\left[\frac{w_{01}}{a_{10}}-1\right] \tag{21}$$

is introduced. It was shown elsewhere that in the case of the constructed low-dimensional model for the vortex street dynamics the $w_{i0}uG^k$ terms are suitable for the calculation of the control signal [10]. For our investigation the coefficient w_{10} was calculated with

$$w_{10}=a_{10}+\beta_{10}a_{10} . \tag{22}$$

Then the energy transfer ΔE to the controlled system is given by

$$\Delta E=\begin{cases}>0 & \text{for } \beta_{10}<0\\ =0 & \text{for } \beta_{10}=0\\ <0 & \text{for } \beta_{10}>0.\end{cases} \tag{23}$$

1. *Increase of the width of the wake region*

In this section the goal dynamics is defined by an increase of the velocity amplitude, i.e., an increase of the width of the wake region. Therefore a negative control parameter was chosen [Eq. (23)]. Figure 12 shows the numerical simulation of the control of the vortex street at Re=67 and the applied control signal calculated from Eq. (20), where $\beta_{10}=-0.005$. When the control is switched on at $t=0.8$ s, the system is entrained, and its phase locks into the phase of the control signal after some oscillations. The state of the goal dynamics is reached at about $t=1.1$ s. When the control is switched off at $t=1.6$ s the system immediately converges back to its natural amplitude. The interesting fact of this simulation is that the mean value of the amplitude of the time signal is shifted to a higher value. This is due to the control signal, where the forcing function fluctuates around a nonzero value of $\overline{U(t)}=3200$. The mean value of $\overline{U(t)}$ depends strongly on the dynamical state of the vortex street (i.e., on the Reynolds number) and on the preselected dynamics. The problem for an experimental application is that such a force cannot be produced by the simple loudspeaker arrangement.

To investigate the applicability of the nonfeedback control theory with this experimental arrangement, the goal dynamics and the corresponding driving force have to be modified. Such a modification is done in two steps. In the first step, the forcing function $F(t)$ is shifted from the nonzero mean value of Fig. 12 to $\overline{F(t)}=0$. The resulting force and its application to the model equation [Eq. (2)] discussed in Fig. 12 are presented in Fig. 13. The time signal of the simulated vortex street now shows a nonlinear modulation, which indicates that the amplitude of the modified force is too small and therefore does not match the physical properties of the vortex street governed by the chosen goal dynamics. In the second step, the modified forcing function is multiplied by a factor of 3.5. Then the nonlinear modulation disappears and the goal dynamics is accomplished. This process is illustrated in Fig. 14, where the same model equation [Eq. (2)] as the one in Figs. 12 and 13 is stimulated by the driving force shown below. The corresponding experimental time signal using the same force is presented in Fig. 15. Taking the physical phenomena for the variation of the width of wake region into account, both experimental response and numerical simulation from Eq. (2) are quantitatively in a good agreement. The problem concerning the scaling of the control signal will be discussed below in a special subsection. Here we will only focus on the general applicability of the control mechanism.

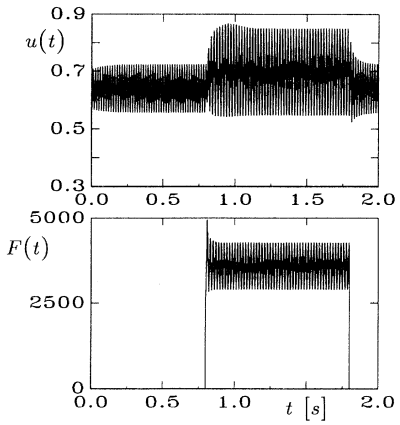

FIG. 12. Numerical simulation of an increase in amplitude of the vortex street at Re=100 (top) and the applied control signal $F(t)$ (bottom). The control signal was calculated from Eq. (20), where $\beta_{10}=-0.005$.

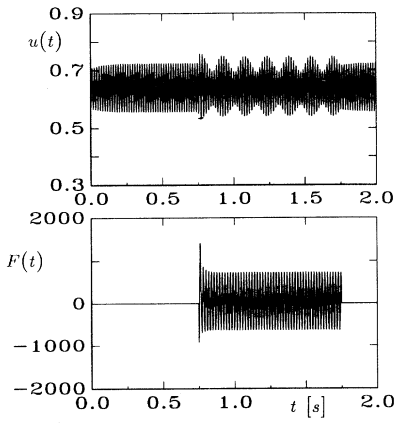

FIG. 13. Same as Fig. 12, but here the applied control signal $F(t)$ is shifted around the mean value of zero by $F(t)=F(t)-\overline{F(t)}$.

2. *Decrease of the width of the wake region*

In technical and engineering applications, one goal of the wake flow control is a total suppression of the vortex street. For technical reasons this goal dynamics is of great importance since the drag of a body in a fluid strongly depends on such wake phenomena. In the following, the possibility of achieving a decrease in amplitude or a suppression of the vortex street is discussed. To achieve a decrease or a total suppression of the vortex

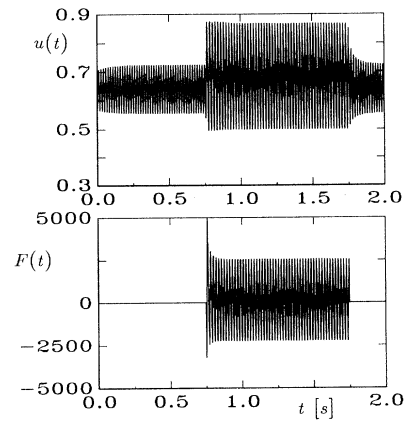

FIG. 14. Same as Fig. 13, but here the applied control signal was multiplied by a factor of 3.5.

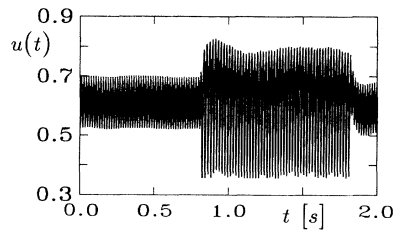

FIG. 15. Experimental time signal of a controlled vortex street at Re=100. This experimental result corresponds to the numerical simulation of Fig. 14.

street, the control parameter β_{10} must be positive [Eq. (23)].

The top of Fig. 16 shows the numerical time signal of a vortex street at Re=100, stimulated by the control signal calculated from Eq. (20). The goal dynamics here is defined by a total suppression of the velocity fluctuations, for which a control parameter $\beta_{10}=0.06$ was chosen. The control started at $t=0.5$ s. It was found that the simulated dynamics of the vortex street locks into the phase of the control signal and is entrained to the selected stationary dynamics. The forcing function applied here possesses two important features. First, the values of $F(t)$ are always negative, and second, $F(t)$ converges to a constant nonzero value in a finite time interval depending on the amplitude-frequency coupling. If such a force is considered to drive the vortex street in the experiment, it is obvious that such a forcing function cannot be produced by the loudspeaker arrangement. Therefore the control fails, even when only a decrease in amplitude is defined by the goal dynamics. Similar to the procedure discussed for an increase in amplitude the calculated force must also be modified.

Figure 17 shows a numerical simulation of a driven vortex street at Re=100, where the goal dynamics is defined by a decrease of the width of the wake region. The driving force shown below is calculated from Eq.

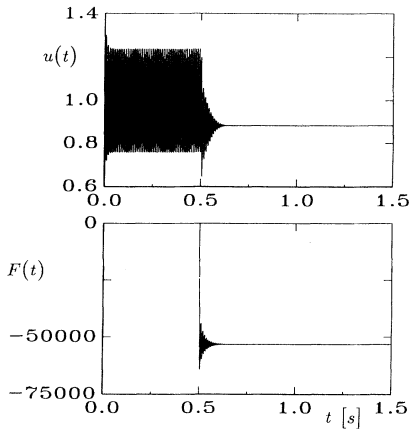

FIG. 16. Numerical simulation of the suppression of a vortex street at Re=100 (top), and the control signal $F(t)$ (bottom). The driving force was calculated from Eq. (20), where $\beta_{10}=0.06$.

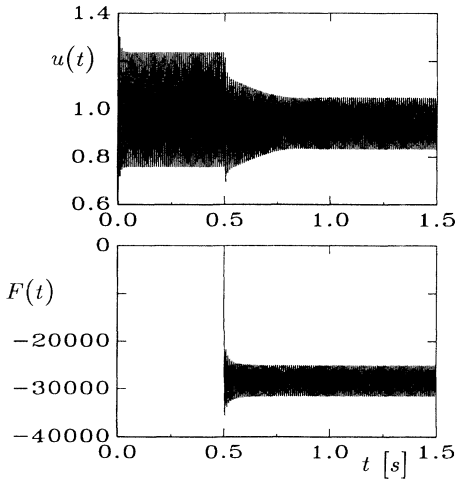

FIG. 17. Numerical simulation of a controlled vortex at Re = 100. The goal dynamics is defined by a decrease of the amplitude $u(t)$. The driving force is calculated from Eq. (20), where $\beta_{10}=0.02$.

(20), where $\beta_{10}=0.02$. It can be seen in the numerical simulation that, due to the appropriate driving force, the goal dynamics is accomplished. Since this control signal cannot be transferred by the loudspeaker arrangement, $F(t)$ was modified in a similar way to one calculated for an increase of the width of the wake region. With the application of such a driving force, the experimental time signal (top) and the corresponding numerical simulation (middle) presented in Fig. 18 are found. The modified

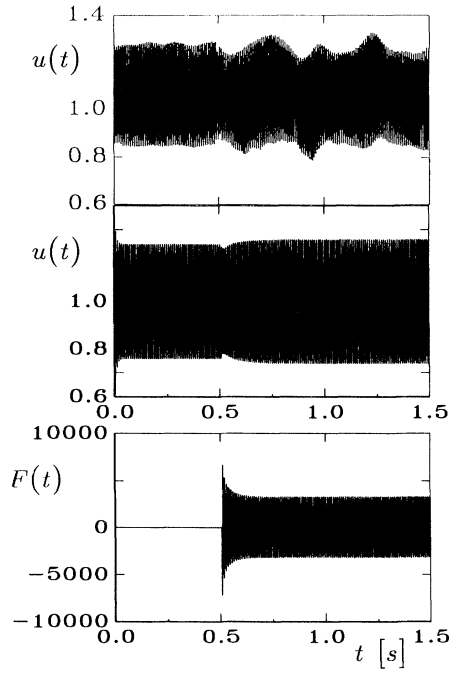

FIG. 18. Experimental (top) and numerical time signal (middle) of a controlled vortex at Re=100 using the modified control force shown below. The driving force is calculated from Eq. (20), where $\beta_{10}=0.02$.

force is shown at the bottom of Fig. 18. Using this type of modified driving force, large deviations of both the experimental and model systems from the goal dynamics can be obtained. This result indicates that another experimental arrangement must be developed which can translate without any modifications (i.e., scaling), the calculated driving forces to the separated vortex street, thereby achieving the preselected dynamics.

V. IMPROVEMENTS OF THE WAKE CONTROL

A. Physical properties of the control functions

In general the external sound excitation is a simple but effective experimental method to stimulate or stabilize the wake flow behind bluff bodies [36,37]. Unfortunately, this experimental control apparatus possesses some physical problems for the nonfeedback control mechanism, because in some cases the exact transfer of the calculated control functions is not possible. In addition, the influence of the sound signal on the development of the vortices in the near wake behind the cylinder is not well known. In the following we discuss in detail the physical properties of the wake control, especially the connection between the main (incompressible) flow field $\vec{U}(\vec{x},t)$ and the secondary flow field $\vec{U}_S(\vec{x}_s,t)$ produced by the external sound excitation.

The secondary flow field $\vec{U}_S(\vec{x}_s,t)$ can be measured in front of the membrane of a loudspeaker using hot-wire anemometry. Here the mean velocity $u_{s,\infty}$ depends on the chosen frequencies and the corresponding amplitudes $F(t)$. The scaling of the control functions depends on the transfer function of the loudspeaker signal, i.e., the factor n of $\vec{U}(\vec{x},t)$ and the secondary flow field $\vec{U}_S(\vec{x}_s,t)$, where $u(t)=nu_s(t)$ and $u_s(t)$ are the velocity fluctuations of $\vec{U}_S(\vec{x}_s,t)$. A successful control can be achieved when the flow field $\vec{U}_S(\vec{x}_s,t)$, governed by the appropriate frequency and amplitude, fits the physical conditions of the preselected dynamics of the wake flow. It is obvious that the effect of $\vec{U}_S(\vec{x}_s,t)$ on the wake flow is not focused on one local point in space, but on a finite volume including the space around the cylinder and the wake region. Surprisingly, the predictions from the constructed model [Eq. (2)] resulting from a measurement at one local point in space (ξ,η) are in very good agreement with the experimental investigations. This is due to the strong correlation of the control parameters of a dynamical system such as the velocity, pressure, etc. [38].

A physical interpretation of the successful control of the vortex street is given as follows: The experiment shows that $\vec{U}_S(\vec{x}_s,t)$ has a strong impact on the pressure field around the cylinder, and therefore on the development of the vortex street in the near wake. After the vortices are developed, they move downstream through the convectively unstable regions in which the influence of $\vec{U}_S(\vec{x}_s,t)$ of the global dynamics of the vortex street is very small. This is consistent with physical intuition, since it appears to be difficult to drive the fully developed complex structure of the vortex street to a preselected structure [10,37]. In conclusion, the good agreement between numerical and experimental results indicates that there might exist a simple relation between the pressure field around the cylinder and the flow field in the near wake of the cylinder.

B. Modified experimental setup

Taking the above mentioned physical principles for the control of the vortex street into account, an experimental arrangement for the control should include several possibilities for the experimentalist. First, a measurement of the fluctuations of the considered variable x_i is of importance, since the calculated control functions are determined by a low-dimensional model [Eq. (2)] which is constructed from the experimental data. Second, the control function $F(t)$ should be directly applied to the vortex street without any modification. Finally, the control should have an effect directly at the place of the development of the vortex street dynamics, i.e., in the absolute sensitive region behind the cylinder. The last argument for the development of an experimental apparatus especially indicates that it is reasonable to shift close to the cylinder the area of the data acquisition and the area of application of the control.

The centerpiece of our arrangement is a cylindrical pipe which replaces the natural cylinder. Figure 19 sketches the experimental bluff body arrangement. The main idea for the bluff body is based on the possibility of measuring and controlling the pressure fluctuation $p(t)$ in the boundary layer of the cylinder. This can be done using a distribution of equidistant pinholes in one plane of the ζ axis at the cylindrical pipe. The number of pinholes and their diameter depend on the inner diameter of the cylindrical pipe and the aspect ratio l/d, i.e., the relation between the outer diameter of the pipe and the length of the cylinder. To suppress a three-dimensional vortex pattern along the ζ axis, such as oblique vortex shedding with certain shedding angles, both ends of the cylindrical pipe are equipped with specially designed end-

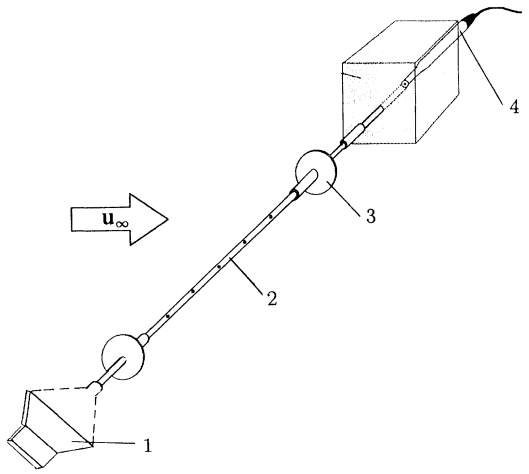

FIG. 19. Schematic presentation of the modified experimental setup. (1) Control apparatus. (2) Cylindrical pipe with n pinholes. (3) Endplates with endcylinders. (4) Pinhole microphone.

plates and endcylinders [39]. To measure the internal pressure fluctuations, a pinhole microphone is placed at one end of the pipe. With the experimental arrangement a control can be achieved by the use of an apparatus placed on the other side of the cylindrical pipe, which periodically or aperiodically inhales or exhales air in and out of the pipe through the pinholes.

To illustrate the potential of the experimental setup, some investigations are presented for a cylindrical pipe of $d=1.5$ mm with two endplates and endcylinders and an l/d ratio of 120 between both endcylinders was mounted in front of the nozzle exit. The circular pipe was equipped with six pinholes of a diameter of 0.7 mm and a mutual distance of 20 mm. Investigations with this bluff body arrangement show that the global shedding axis is parallel to the ζ axis of the cylindrical pipe from which the pressure fluctuations $p(t)$ can be accurately measured. From such measured time signals, a model similar to the constructed model for the velocity fluctuations [Eq. (2)], i.e.,

$$\ddot{p}=\sum_{\substack{i=0,\ldots,3\\ j=0,\ldots,3-i}} c_{ij}p^i\dot{p}^j\,, \tag{24}$$

can be derived [38,40].

The coefficients c_{ij} of the model reconstructed from the pressure fluctuations of a vortex street at Re=100 and the corresponding coefficients a_{ij} of the model for the velocity fluctuations are shown in Table I. It can be seen that some of the coefficients have similar values. Furthermore, it is found by a numerical integration that the normalized limit cycle of the trajectory of the velocity and the pressure fluctuations are in a good agreement [41].

The essential physical properties of the wake flow which enables the calculation of the optimal forcing function as well as accurate parameters for a stability analysis can be determined easily from the reconstructed model coefficients. It has been shown elsewhere [10,26] that a very useful tool for the estimation of the quality of the reconstructed model and the analysis of its model coefficients is based on the following idea: For slowly varying amplitudes and frequencies, the general oscillator equation [Eq. (2)] can be approximated by the Landau equation

$$\dot{r}=\alpha r-\beta r^3,\quad \dot{\varphi}=-\gamma-\delta r^2\,,$$

where r is the amplitude and $\omega:=\dot{\phi}$ is the angular frequency. The corresponding Landau coefficients can be calculated from

$$\begin{aligned}&\alpha=\tfrac{1}{2}a_{01},\quad \beta=-\tfrac{1}{8}(a_{21}+3a_{03})\,,\\ &\gamma=\tfrac{1}{2}(1-a_{10}),\quad \delta=-\tfrac{1}{8}(a_{12}+3a_{30})\,.\end{aligned} \tag{25}$$

The resulting Landau coefficients of Table I for both the velocity $u(t)$ and pressure fluctuation $p(t)$ are shown in Table II. The coefficient α is a measure for the instability of the fixed point $r=0$, and $\beta>0$ defines the damping of the oscillator at large amplitudes. Since the data have been normalized, the angular frequency $w_g=1$ and the amplitude of the limit cycle $r_g=1$, where $r_g=(\alpha/\beta)^{1/2}$, and therefore $\alpha=\beta$. The value of γ represents the angular frequency for small amplitudes, whereas δ describes the increase of the frequency for a corresponding increase of the amplitude.

The Landau coefficient β calculated from the reconstructed coefficients of the pressure fluctuations shows a larger value compared to the velocity fluctuations. This means a faster transition to the asymptotic solution, whereas the deviation of the amplitude-frequency coupling (δ) for the pressure and the velocity is very small, which characterizes an essential physical property for the nonfeedback control or a nonlinear resonant stimulation. These results indicate that it is possible to measure the pressure fluctuation via our experimental arrangement and, therefore, a very effective application of the nonlinear nonfeedback method can be expected.

VI. DISCUSSION

This section will discuss the physical insight of the model-based control and its applicability to technical wake flows, i.e., wakes at higher Reynolds numbers. The nonlinear nonfeedback control strategy can be taken as a generalization of the linear notion of driving the systems by out of phase forcing. The physical interpretation of the calculated driving force is that the forcing simply cancels the undesirable dynamics and imposes the preselected one. Even though the goal dynamics cannot be chosen arbitrarily, several experiments have proven that the range of specific behavior can be very wide (for details, see Keefe [9]).

The dynamical properties of the entrainment of nonlinear systems to periodic motion at certain frequencies

TABLE I. Comparison of the reconstructed coefficients of the velocity $a_{ij}(u)$ and pressure fluctuations $c_{ij}(p)$ for a vortex street at Re = 100.

i	j	$a_{ij}(u)$	$c_{ij}(p)$
0	0	0.0000	0.0000
0	1	0.1493	0.2595
0	2	−0.0301	0.1443
0	3	−0.1367	−0.2316
1	0	−1.0000	−1.0000
1	1	0.4203	0.5175
1	2	0.0263	0.0264
2	0	−0.1444	−0.1421
2	1	−0.1873	−0.3432
3	0	−0.0691	−0.0719

TABLE II. Landau coefficients of Eq. (24) for the coefficients of Table I.

	$u(t)$	$p(t)$
α	0.0747	0.12975
β	0.0747	0.1298
γ	1.0000	1.0000
δ	0.0226	0.0237

based on its nonlinearity or amplitude-frequency coupling is well known. On the other hand, the nonlinear control method indicates that the ability of a nonlinear system to be entrained to a preselected motion is much more general [1]. The crucial point here is that the overall success of a model-based control of nonlinear systems, such as wake flows, can be attributed to how accurate characteristic physical properties can be predicted from the low-dimensional model reconstructed from the experimental system. In this context arises the questions of why the nonlinear model-based control strategy might be advantageous for the bluff body wake control.

In earlier works concerning active control mechanism, such as an oscillating cylinder, the limitation of the control of wake flows was discussed using ideas of linear stability theory. The suppression of the vortex street near the onset of global instability by single sensor-single actuator feedback control in the wake of an oblong cylinder was discovered by Berger [42,43] to be difficult, and only possible very close to the natural critical Reynolds number, i.e., $\mathrm{Re} \leq 80$. Furthermore, Monkewitz [44] has shown that, to induce global instability, only a single and, in most applications, unspecified global mode has to be destabilized. The suppression of global instability implies that all global modes have to be attenuated. In general one cannot assume that a single sensor is sufficient to handle multiple global modes, which often have very closely spaced frequencies and occur at higher Reynolds numbers, i.e., $\mathrm{Re} > 160$. Therefore if the forcing functions do not fit perfectly to the overall dynamical behavior of the wake flow, the driving force controls one mode but might destabilize other ones and thereby defeat its purpose. Huerre and Monkewitz [45] speculated that in all examples in which a simple single sensor-single actuator feedback control works, there was only a single, self-excited global mode to control, with all other modes strongly damped. This statement is in a good agreement with the results of the nonlinear nonfeedback control presented here.

In comparison with the traditional linear control methods, the nonlinear forcing is advantageous, since the dynamics of the vortex street is nonlinear and therefore its energy transfer is more effective [46]. For Reynolds numbers very close to the critical Reynolds numbers, i.e., $45 \leq \mathrm{Re} \leq 80$, the amplitude-frequency coupling is very weak. Therefore, similar results for the control using linear or nonlinear driving forces can be obtained [47]. For higher Reynolds numbers the coupling between the natural amplitude and frequency is increased, leading to a stronger nonlinearity of the calculated forcing functions and a higher efficiency of the nonlinear wake control. Furthermore, due to such an optimal forcing an increase of the region of entrainment, i.e., the regions of a frequency lock in, and the possibility of freezing a large number of degrees of freedom in the transitional range ($160 \leq \mathrm{Re} \leq 300$) can be obtained [48].

From a stability point of view one of the main advantages of the model-based control is that the growth rates of the global mode is determined directly from the reconstructed model equation. Therefore it contains a high degree of physical insight into the global mode characteristics [26], and the energy transfer to the global mode can be assumed to be most efficient. Noise might also play another important role for the stability and quality of most control methods, since it reduces the overall efficiency. Such small stochastic forces from outside the dynamical system have a neglectible influence on the stability of the model-based control, because no feedback is required. On the other hand, the quality of the control can be sensitive to modeling errors in Eq. (2).

An interesting question in the field of mechanical engineering is how such a control strategy can be technically applied to wake flows at high Reynolds numbers. Since the model-based control relies on forecasting techniques using low-dimensional models, the applicability to technical wake flows might be limited to low-dimensional dynamical states. It has been shown by Keefe [9] that the model-based control generally seems to hold potential for transitional flows, but might necessarily have forcing functions requiring energies high compared to the natural dynamics. The greatest problem of the application of a model-based control to transitional or turbulent wakes or other fluid mechanical systems is the complexity of their underlying exact model equations. The synchronization, the stabilization, or the suppression of such complex dynamics of the flow field governed by multiply unslaved modes can only be achieved by a similarly complex forcing function. An additional problem is connected with the time dependence of the three-dimensional spatial structure in the wake behind the bluff body. Furthermore the amplitude of the control force increases rapidly, even when the control is restricted to a small domain such as the absolute sensitive region behind a body [49], or in case of a stabilization of a global mode in transitional wakes [48].

A field of interest in wake flow research is the drag reduction of the body by suppressing its vortex shedding. It is already known that the suppression of vortex shedding is connected to the control of the absolute unstable region in the near wake directly behind the bluff body [45,49]. In such regions the introduced disturbances spread upstream and downstream and contaminate the entire parallel flow. Since wake flows behave like oscillators, the evolution of vortices does not rely on the spatial amplification of external perturbations but rather on the growth of initial disturbances in time.

With the model-based control, a total suppression of the vortex street and a stabilization of the transitional or turbulent wakes which, for example, lead to an improvement of the signal-to-noise ratio and can be useful in the field of data acquisition, are of particular interest. The stabilization of the vortex street can be achieved by the loudspeaker arrangement used here (see, for example, [37]), but the efficiency of the control decreases with the increase of Reynolds number, due to the increase of the complexity of the wake flow [41]. For the effective suppression of the vortex street by suction or blowing via this type of control, some assumptions have to be introduced. The basic idea is to calculate the lowest level of suction or blowing needed for a total suppression of the velocity fluctuation of the vortex street, i.e., to prevent the development of vortex shedding. In the first step we

assume that even though the wake at higher Reynolds numbers is turbulent and the corresponding underlying dynamics is high dimensional [37], the near wake is governed by a single global mode, i.e., by a low-dimensional oscillator with only one characteristic eigenfrequency. All other active modes will be neglected in the later analysis. In the next step, the experimental data are analyzed to extract the characteristic dynamical behavior of the global mode, from which a low-dimensional model equation can be reconstructed [50]. If the global mode characteristics can be modeled with a certain accuracy, then a forcing function similar to the one presented in Fig. 16 can be calculated. Preliminary investigation indicates that this simplified ansatz might be very successful in estimating the appropriate suction or blowing level. The advantage of this approach is that the lowest level of suction or blowing necessary for the suppression of vortex shedding can be easily calculated. This is due to the fact that the forcing function is started near resonance, with an appropriate amplitude at which a large number of active modes will be damped out rapidly. Then the dynamics of the vortex shedding will be entrained by the forcing function up to the dynamical state of preventing the development of a vortex street. Note that the assumption of the accurate approximating a high-dimensional wake flow by a simple model with only one global mode can only be applied for this type of preselected dynamics. For other preselected dynamics the initial trajectory, including the global and all other additional modes, must be considered. A further advantage of the model-based control is that, if the model coefficients have a predictable dependence on the velocity u, a long time suppression can be achieved by an adaptive model-based control mechanism [24]. Here the response of the experimental system is measured from time to time in order to update the model coefficients.

For the exact physical interpretation of the wake flow control a detailed knowledge of the connection between regions of absolute instability and global flow response is of great interest. Especially from an experimental point of view there still exists only little evidence that the control of global modes must be applied in or near regions where local linear theory predicts absolute instability (see, for example, Refs. [45,51]). However, a complete experimental confirmation of this interpretation of the flow response to external driving forces and its comparison to results of a local linear stability analysis is not available. Here the difficulties are based mainly on the complexity of an appropriate experimental setup and the measurement of the interested physical properties of the considered wake region. Furthermore, the accurate determination of the corresponding model coefficients needed for a mathematical analysis is still an open problem [41,52,53]. With the modeling ansatz discussed here, a physical and mathematical analysis of the reconstructed low-dimensional model [Eq. (2)] in connection with a study of its coefficients a_{ij} for varying control parameters can be carried out, and may confirm the predictions of the local linear theory [33,41]. In particular, the investigation of the reconstructed model coefficients a_{ij} with dependence on control parameters such as the Reynolds number and the location of observation (ξ,η) in the wake of the body, has provided physical insight into the vortex street dynamics. Therefore, the reconstruction of accurate model parameters from experimental data of the vortex street dynamics enables a much more detailed look into its global flow characteristics and its nonlinear phenomena [41,53].

VII. SUMMARY

In this work we have studied the possibility of a nonlinear resonant stimulation and a nonfeedback control of the periodic cylinder wake. We have shown that with the nonlinear resonant stimulation the width of the wake region can be increased or decreased. In addition, a long-term decrease of the width of the wake region of approximately 15% can be achieved by a modification of the standard nonlinear forcing functions. Neither a short- nor long-term decrease of the width of the wake region is possible with sinusoidal driving forces. Taking the physical aspects of the resonantly stimulated vortex street into account, a very good qualitative agreement between the experiment and numerical predictions from an extracted low-dimensional model was found. In the case of the nonfeedback control of the vortex street, a good qualitative agreement between experiment and numerical simulation was found for an increase of the width of the wake region. Since the forcing functions resulting from the nonfeedback control algorithm cannot be exactly transferred by a loudspeaker arrangement, a decrease in amplitude or a total suppression of the vortex street could not be achieved. In general, with the loudspeaker arrangement used in this work, the nonlinear control works best when the preselected or goal dynamics rearranges the energy of the uncontrolled flow into another nonlinear form, instead of simply suppressing the vortex street. Note that, in the case of the numerical simulation, a decrease of the width of the wake region or a total suppression of the vortex street in general seems possible, but it requires a different control apparatus. Therefore, an experimental control mechanism was proposed which can translate the calculated forcing function to the experimental system in order to achieve the preselected dynamics. In conclusion, the model-based control possesses some interesting potential for the control of wake flows behind bluff bodies, but further improvements of the general method as well as the experimental implementation are needed. Developments and investigations along these lines are in progress.

ACKNOWLEDGMENTS

The authors would like to thank H. Eckelmann, E. A. Müller, and D. Ronneberger, and in particular Chr. Heck for many stimulating discussions. We are indebted to Nick Weber for reading the manuscript and making helpful suggestions.

APPENDIX

An example for a set of physical and normalized coefficients reconstructed from experimental data of a vortex street at Re = 65 and 100 used for the numerical

TABLE III. Physical and normalized coefficients of the reconstructed model equation [Eq. (2)] of a vortex street at Re = 65. The unit of the physical coefficients a_{ij} is $m^{1-i-j}s^{i+2j-2}$.

a_{ij}	Physical	Normalized
a_{00}	+319 604.094 328 001 5	−0.0001
a_{01}	−3059.043 461 279 081	+0.0323
a_{02}	−17.937 410 898 698 39	+0.0476
a_{03}	−1.009 903 326 994 349 3E −02	−0.0303
a_{10}	−1 046 168.439 787 224	−1.0825
a_{11}	+8831.244 519 847 463	+0.2117
a_{12}	+29.172 819 836 864 54	+0.2363
a_{20}	+1 147 522.678 679 479	+0.1769
a_{21}	−6287.034 585 214 860	−0.1374
a_{30}	−462 000.921 322 778 7	−0.0272

TABLE IV. Physical and normalized coefficients of the reconstructed model equation [Eq. (2)] of a vortex street at Re = 100.

a_{kl}	Physical	Normalized
a_{00}	+716 633.580 534 967 6	+0.0000
a_{01}	−3225.430 010 905 253	+0.1493
a_{02}	−0.577 418 745 018 789 4	−0.0310
a_{03}	−3.469 377 722 252 013 2E −03	−0.1367
a_{10}	−1 505 338.262 742 434	−1.0000
a_{11}	+5429.853 560 900 833	+0.4204
a_{12}	+0.445 392 807 193 977 6	+0.0263
a_{20}	+1 314 175.151 508 925	−0.1444
a_{21}	−2116.555 265 886 052	−0.1873
a_{30}	−521 043.861 420 737 0	−0.0691

simulation are presented in Tables III and IV, respectively. The double precision format of the physical coefficients is necessary for the numerical investigation, because of the large differences between the various magnitudes.

In order to permit a mathematical analysis, the reconstructed model equations [Eq. (2)] must be normalized so that the attractor is close to a unit circle with the origin as its center. The angular velocity on the circle should be nearly unity. The corresponding coefficients are said to be normalized. More details of the normalization process can be taken from Ref. [26].

[1] A. Hübler and E. Lüscher, Naturwissenschaften **76**, 67 (1989); A. Hübler, in *Modeling Complex Phenomena,* edited by L. Lui and V. Naroditsky (Springer, New York, 1992), p. 5.

[2] E. A. Ott, C. Greboggi, and J. A. Yorke, Phys. Rev. Lett. **64**, 1196 (1990).

[3] B. D. O. Anderson, *Stability Analysis of Adaptive Systems: Passive and Averaging Analysis* (MIT Press, Cambridge, MA, 1986).

[4] I. M. Y. Mareels and R. R. Bitmead, IEEE Trans. Circuits Syst. **35**, 835 (1988).

[5] F. M. A. Salam and S. Bai, IEEE Trans. Circuits Syst. **35**, 842 (1988).

[6] B. A. Hubermann and E. Lumer, IEEE Trans. Circuits Syst. **37**, 547 (1990).

[7] A. Hübler, Dissertation, Technischen Universität Müchen, 1987.

[8] R. Shermer and A. Hübler, Phys. Rev. A **43**, 5642 (1991).

[9] L. R. Keefe, Phys. Fluids A **5**, 931 (1993).

[10] F. Ohle, Dissertation, Max-Planck-Institut für Strömungsforschung, Göttigen, 1992.

[11] R. Georgii, W. Eberl, A. Hübler, and E. Lüscher, Helv. Phys. Acta **62**, 290 (1989).

[12] B. Rückerl, W. Eberl, A. Hübler, and E. Lüscher, Helv. Phys. Acta **61**, 80 (1988).

[13] F. Ohle and H. Eckelmann, *IUTAM-Symposium on Bluff Body Wakes, Dynamics, and Instabilities* (Springer, Heidelberg, 1993), p. 241.

[14] W. L. Ditto, S. N. Rauseo, and M. L. Spano, Phys. Rev. Lett. **65**, 3211 (1990).

[15] R. Roy, T. W. Murphy, T. D. Maier, A. Gills, and E. R. Hunt, Phys. Rev. Lett. **68**, 1259 (1992).

[16] E. R. Hunt, Phys. Rev. Lett. **67**, 1953 (1991).

[17] A. Garfinkel, M. L. Spano, W. L. Ditto, and J. N. Weiss, Science **257**, 1230 (1992).

[18] B. Hübinger, R. Doerner, W. Martienssen, M. Herderring, R. Pitka, and U. Dressler, Phys. Rev. E **50**, 932 (1994).

[19] N. H. Packard, J. P. Crutchfield, J. D. Farmer, and R. S. Shaw, Phys. Rev. Lett. **45**, 712 (1980).

[20] A. J. Cremers and A. Hübler, Z. Naturforsch. **42a**, 797 (1987).

[21] D. S. Broomhead and G. P. King, Physica D **20**, 217 (1986).

[22] J. D. Farmer and J. J. Sidorowich, Phys. Rev. Lett. **59**, 845 (1987).

[23] J. P. Crutchfield and B. S. McNamara, Complex Syst. **1**, 417 (1987).

[24] F. Ohle, A. Hübler, and M. Welge (unpublished).

[25] J. L. Breeden and A. Hübler, Phys. Rev. A **42**, 5817 (1990).

[26] B. Noack, F. Ohle, and H. Eckelmann, Physica D **56**, 389 (1992).

[27] J. Guckenheimer and Ph. Holms, *Nonlinear Oscillations, Dynamical Systems, and Bifurcations of Vector Fields, Applied Mathematical Science* (Springer, New York, 1983), p. 42.

[28] J. D. Farmer and J. J. Sidorowich, Physica D **47**, 373 (1991).

[29] G. Reiser, A. Hübler, and E. Lüscher, Z. Naturforsch. **42a**, 803 (1987).

[30] Chr. Wargitsch and A. Hübler, Phys. Rev. E **51**, 1508 (1995).

[31] *Bluff Body Wakes, Dynamics, and Instabilities,* edited by H. Eckelmann, M. Graham, P. Huerre, and P. Monkewitz (Springer, Heidelberg, 1993).

[32] F. Ohle, P. Lehmann, E. Roesch, H. Eckelmann, and A. Hübler, Phys. Fluids A **2**, 479 (1990).

[33] F. Ohle and H. Eckelmann, Phys. Fluids A **4**, 1707 (1992).

[34] M. Brede, F. Ohle, and H. Eckelmann, Z. Angew. Math. Mech. **74**, T491 (1993).

[35] S. Shi and H. Rabitz, Comput. Phys. Commun. **63**, 71 (1991).

[36] E. Detemple-Laake and H. Eckelmann, Exp. Fluids **35**, 217 (1989).
[37] F. Ohle, Chaos, Solitons Fractals **5**, 1871 (1995).
[38] M. Lange and F. Ohle, Helv. Phys. Acta **68**, 211 (1995).
[39] M. König, H. Eisenlohr, and H. Eckelmann, Phys. Fluids A **2**, 1607 (1992).
[40] Chr. Heck and F. Ohle (unpublished).
[41] F. Ohle, Habilitationsschrift (unpublished).
[42] E. Berger, *Jahrbuch der Wissenschaftlichen Gesellschaft für Luft- und Raumfahrt (DGLR)* (Vieweg, Braunschweig, 1964), p. 164.
[43] E. Berger, Phys. Fluids **10**, 191 (1967).
[44] P. A. Monkewitz (unpublished).
[45] P. Huerre and P. A. Monkewitz, Annu. Rev. Fluid Mech. **22**, 473 (1990).
[46] E. Roesch, F. Ohle, H. Eckelmann, and A. Hübler, *The Global Geometry of Turbulence,* edited by J. Jimenez (Plenum, New York, 1991), p. 11.
[47] F. Ohle (unpublished).
[48] F. Ohle, Chr. Heck, and J. Walter (unpublished).
[49] H. Oertel, Jr. and J. Delfs (unpublished).
[50] Chr. Heck and F. Ohle, Helv. Phys. Acta **68**, 217 (1995).
[51] M. Schumm, E. Berger, and P. A. Monkewitz, J. Fluid Mech. **271**, 17 (1994).
[52] P. Albaréde und M. Provansal, J. Fluid Mech. **291**, 191 (1995).
[53] F. Ohle and Chr. Heck, Helv. Phys. Acta (to be published).